nature energy

Article https://doi.org/10.1038/s41560-022-01189-1

Metal oxide barrier layers for terrestrial and space perovskite photovoltaics

In the format provided by the authors and unedited

Table of Contents

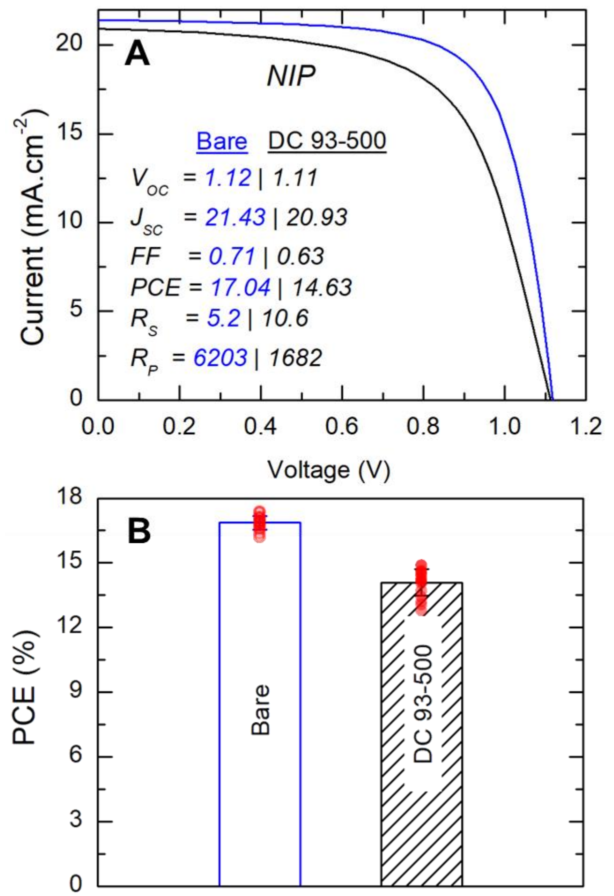

Supplementary Figure 1. Effect of DC 93-500 encapsulation schemes on device performance. The deleterious effect of the space-grade DC 93-500 silicone elastomer encapsulant on *NIP* triple-cation cells. Data in (B) is based on 16 devices for each category which are depicted by red circles overlayed on the bars. Error bars represent standard deviation. While the series resistance (R_S) increases after DC 93-500 encapsulation from 5.2 $\Omega.cm^{-2}$ to 10.6 $\Omega.cm^{-2}$, the shunt resistance (R_P) undergoes a reduction from 6203 $\Omega.cm^{-2}$ to 1682 $\Omega.cm^{-2}$. These changes cause a reduction in the fill-factor (FF). This likely happens because of a chemical or mechanical modification of the device stack upon application of DC 93-500. The silicone elastomer and the solvent can either chemically interact with the device stack or can exert mechanical strain on it during the drying process. Information on the exact chemical composition of this elastomer has not been made readily available by the supplier due to proprietary constraints.

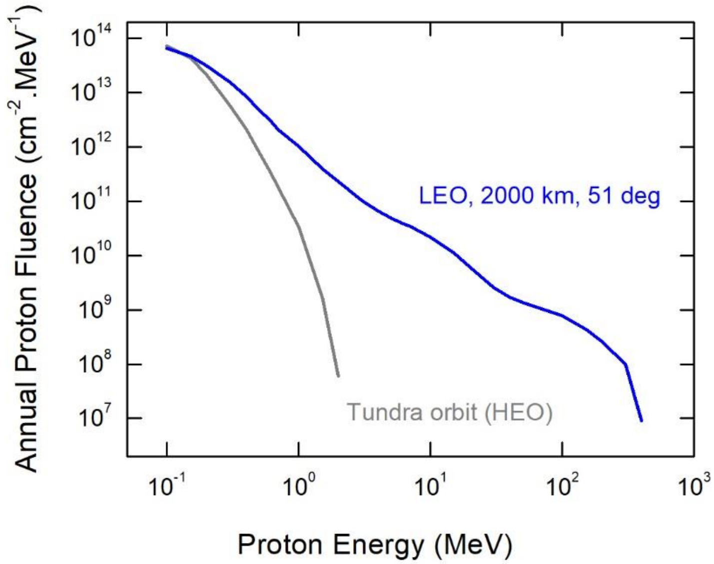

Supplementary Figure 2. Proton environments in LEO and Tundra orbits.
Differential proton fluence for a 1-yr mission in a LEO orbit (blue) and a Tundra orbit (grey).

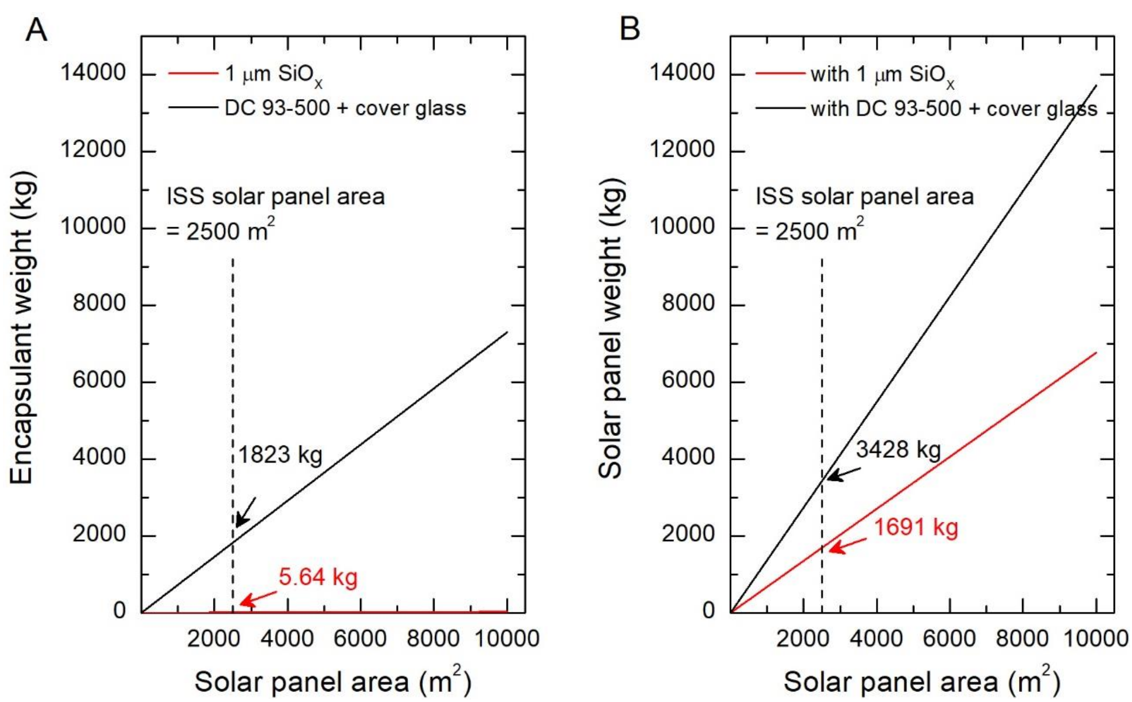

Supplementary Figure 3. Weight benefit of SiO_X encapsulation.
(A) Comparison between encapsulant weights for DC 93-500 and cover glass (black), and 1 μm SiO_X. SiO_X results in 99.7% encapsulant weight reduction. (B) Comparison of perovskite solar panel weights as a function of the panel area using DC 93-500 and cover glass (black), and 1 μm SiO_X (red) encapsulation schemes. Weights were measured on solar cells fabricated on ultrathin Ceria-doped borosilicate glass substrates using the two encapsulation techniques. These weights

were then extrapolated to larger panel areas. An area of 2500 m^2 corresponds to the solar arrays powering the International Space Station (ISS). SiO_X reduces the panel weight by 50.7%.

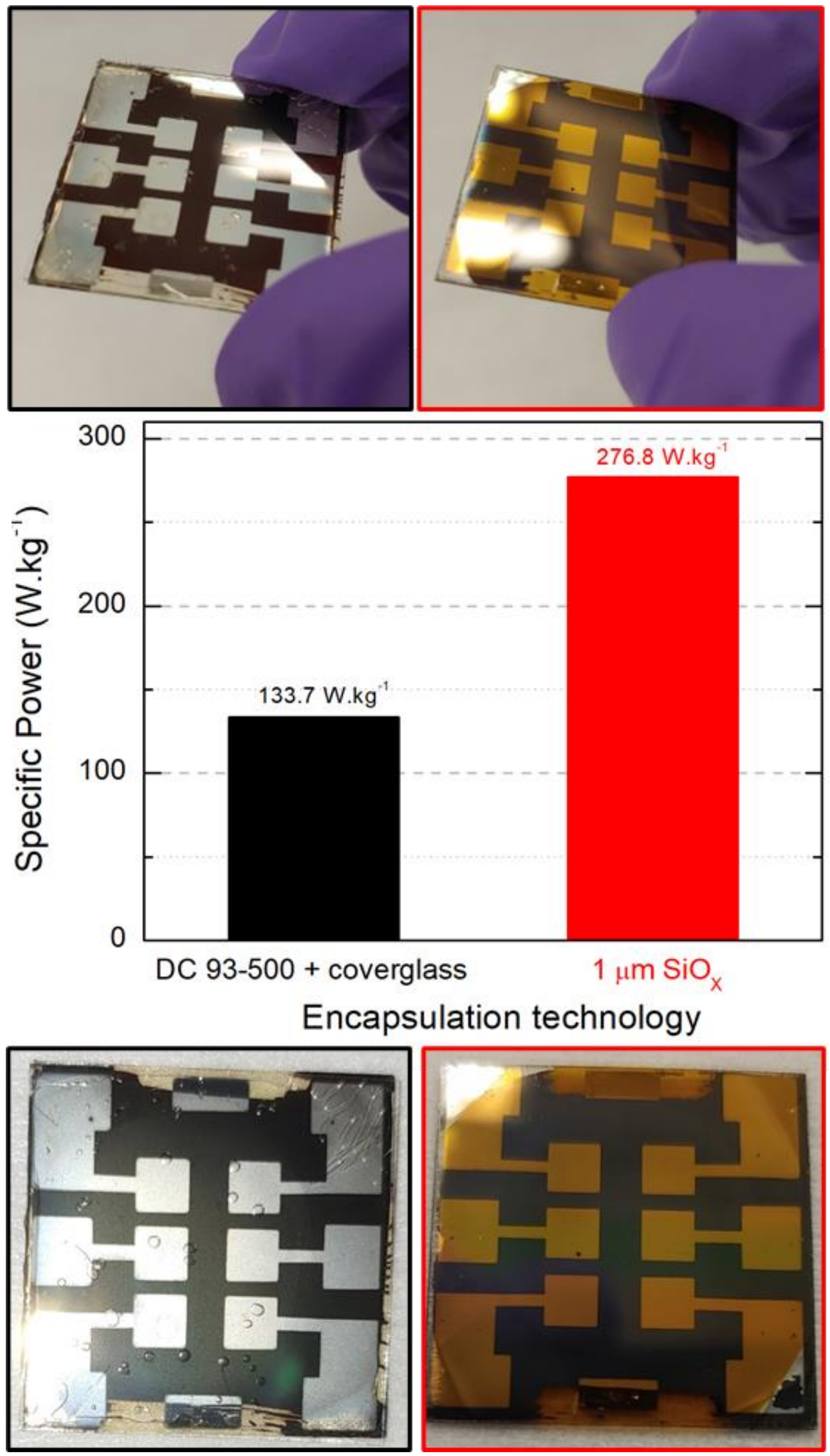

Supplementary Figure 4. Specific power advantage of SiO_X encapsulation.

Specific powers were measured for perovskite solar cells fabricated on lightweight Ceria-doped borosilicate glass substrates 250 μm thickness, using 'DC 93-500 + cover glass' encapsulation scheme (black) and SiO_X scheme (red). Bare cells without any encapsulation were found to weigh ~400 mg. For the DC 93-500 scheme, ~60 mg DC 93-500 was required to fully cover the solar cell. This was then covered with a ~400 mg of Ceria-doped borosilicate cover glass from the top. Despite the care, it is usual for this encapsulation technique to result in air bubbles (see photo) that can cause rupture of cover glass in space due to vacuum. For the SiO_X encapsulation scheme, the weight of 1 μm SiO_X was measured to be 1.45 mg, which is close to the theoretically determined value of 1.37 mg considering a mass density of 2.13 $g.cm^{-3}$. Initial device PCEs were found to be ~18.5%, not considering the slight loss in performance that happens after DC 93-500 encapsulation. Using this output power and factoring in the experimentally measured device weights, a specific power of 133.7 $W.g^{-1}$ was determined for the 'DC 93-500 + cover glass' encapsulated devices. For the SiO_X encapsulated device, a 107% increase in the specific power to 276.8 $W.g^{-1}$ was found. It is important to note here that we ensured full coverage of the cells with the encapsulants without leaving edges exposed for electrical contact. This was done to get a precise estimate on the encapsulant weights.

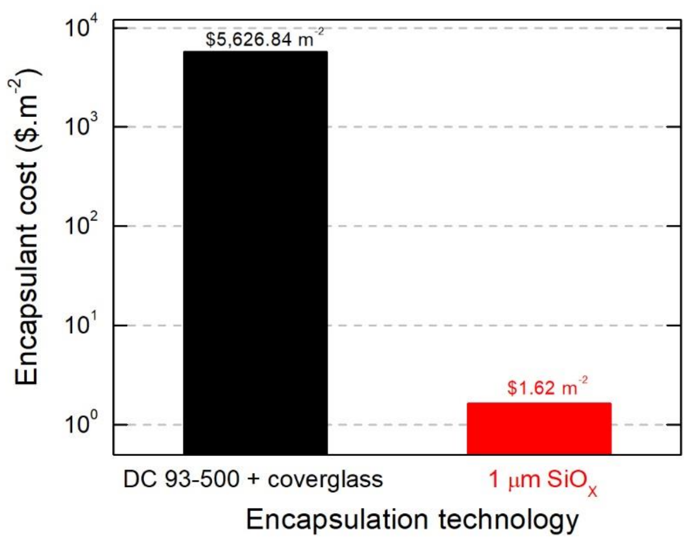

Supplementary Figure 5. Cost benefit of SiO_X encapsulation.

Cost analysis for the 'DC 93-500 + cover glass' and 1 μm SiO_X encapsulation technologies. Price data was acquired from the materials suppliers of DC 93-500, Ceria-doped borosilicate glass, and SiO_X. The cost model considered a square meter of solar panel area and costs of encapsulation material required. SiO_X is found to offer a 99.97% reduction in materials costs. It is expected that the deposition techniques used and the rate of deposition of these encapsulants will further enhance the cost contrasts. While SiO_X can be deposited using the industry-compatible thermal evaporation technique at deposition rates >10 $nm.min^{-1}$, the 'DC 93-500 + cover glass' scheme is a slow process requiring extreme care and time to ensure complete coverage of the device area.

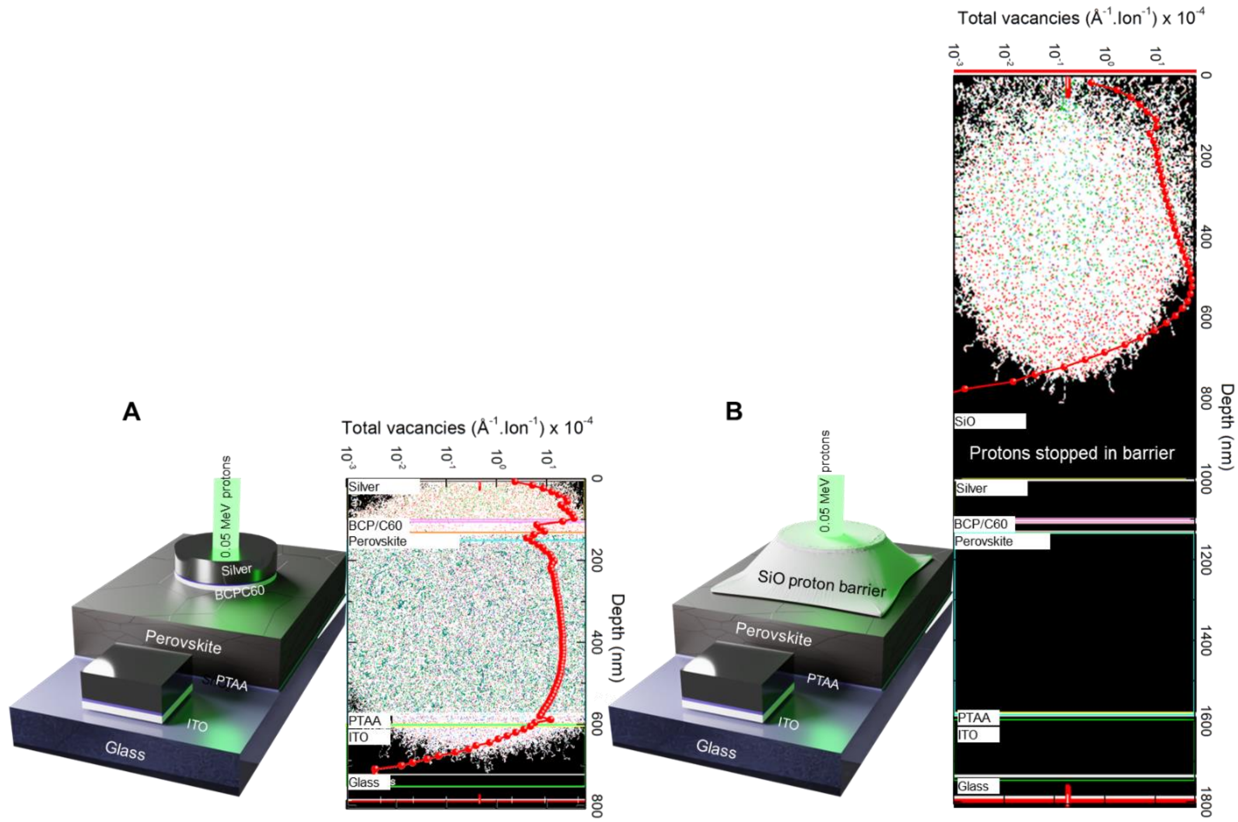

Supplementary Figure 6. SRIM/TRIM simulations for 0.05 MeV protons on *PIN* cells. Theoretical simulations showing interaction of 0.05 MeV protons with a *PIN* triple-cation solar cell (A) without, and (B) 1 μm SiO_X barrier.

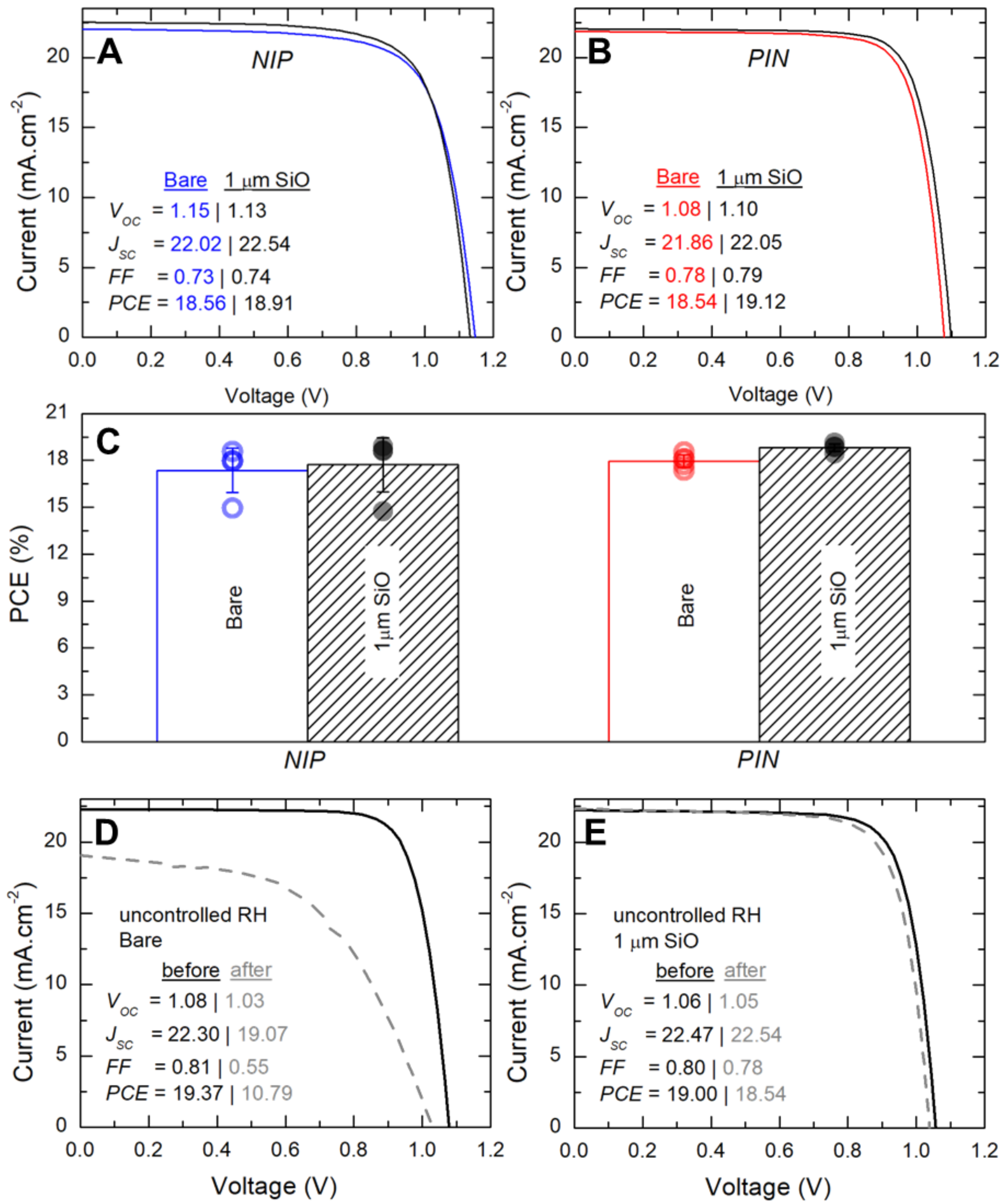

Supplementary Figure 7. Effect of SiO_X encapsulation on device performance.
J-V curves for bare and protected triple-cation solar cells in (A) *NIP*, and (B) *PIN* configuration. (C) Bar graphs showing the effect on PCEs after 1 μm SiO_X deposition. Averages were performed over 4 and 5 devices for the *NIP* and *PIN* cells, respectively, depicted by circles overlayed on the bars. Error bars represent standard deviation. *PIN* solar cells were exposed to an uncontrolled moisture environment for a period of multiple days. While the bare devices underwent degradation, 1 μm SiO_X protected cells showed no noticeable PCE change. *J-V* curves for devices exposed to

uncontrolled moisture and temperature are shown in (D) and (E) for the bare and 1 μm SiO_X protected cells.

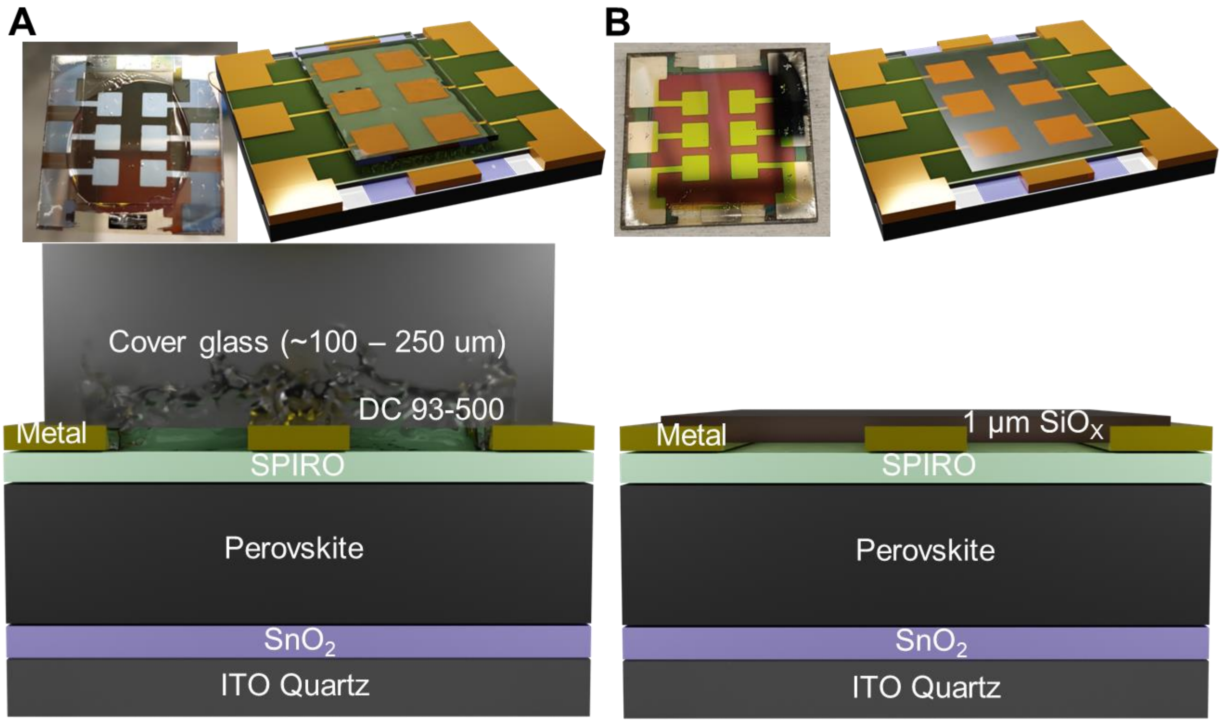

Supplementary Figure 8. Schematic illustration of DC 93-500 and SiO_X encapsulation schemes.
Schematics showing a perovskite solar cell encapsulated with (A) DC 93-500 and cover glass, and (B) with SiO_X barrier. Photos of representative devices are included in insets. Cross-sectional schematics are also shown for each case with the various layers in the device stacks. Light is incident from the quartz side (bottom).

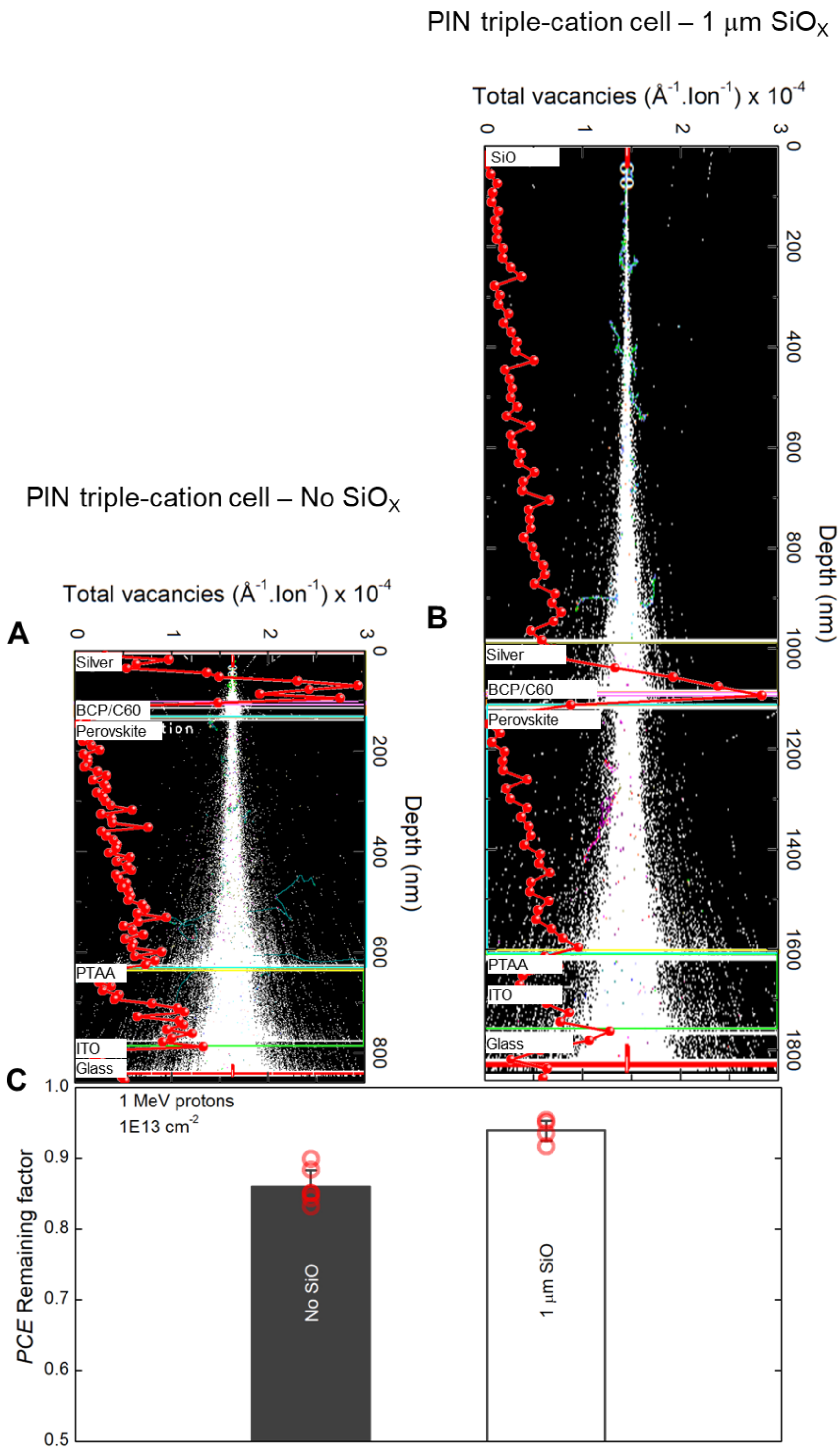

Supplementary Figure 9. SRIM/TRIM simulations for 1.0 MeV protons on *PIN* cells.
1 MeV proton irradiation of PIN triple-cation cells. SRIM/TRIM simulations showing straggling of 1 MeV protons in PIN perovskite solar cells (A) without, and (B) a 1 µm SiO_X barrier. Damage profiles within the solar cell are found to be the same across the two architectures, however, C) an increase in PCE remaining factor is observed for the SiO_X-protected device. Given the high IEL

associated with 1 MeV protons, the bare cell also has a higher remaining factor likely due to the self-healing mechanism involved with IEL. Sample sizes for the 'No SiO' and '1 μm SiO' cells are 6 and 4, respectively. Individual datapoints are depicted by red circles overlayed on the bars. Error bars represent standard deviation.

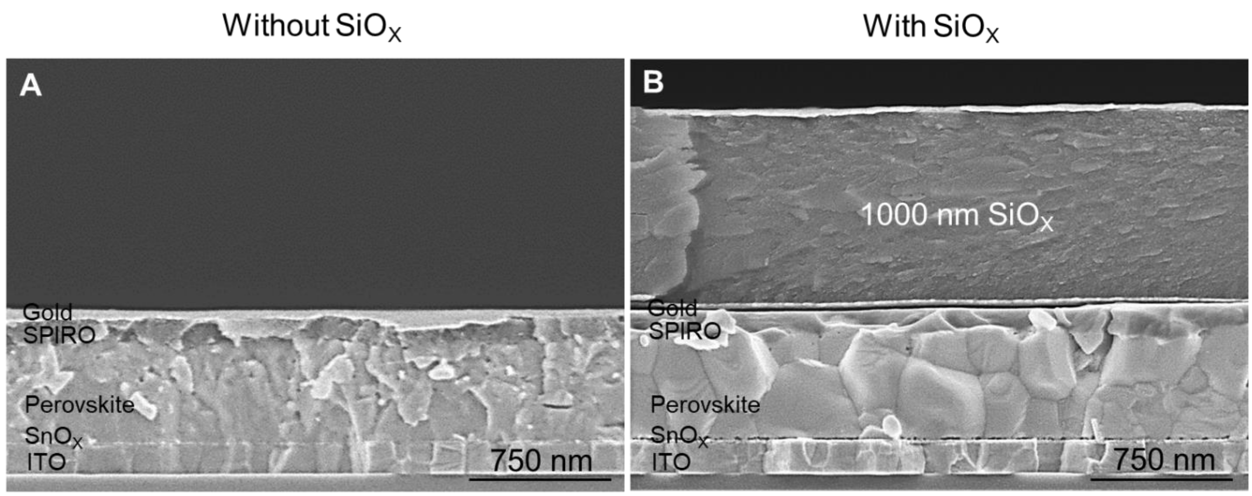

Supplementary Figure 10. X-SEM evidence of proton damage in the device stack.
X-SEM images of *NIP* triple-cation solar cells (A) without, and (B) with SiO_X barrier, irradiated with 0.05 MeV protons at a fluence of 10^{15} cm^{-2}. Proton irradiation leads to severely disrupted microstructure in the bare solar cell, while SiO_X protects the device stack from radiation damage. The bare device showed complete damage (0% PCE), while the SiO_X-capped device showed no drop from its initial PCE.

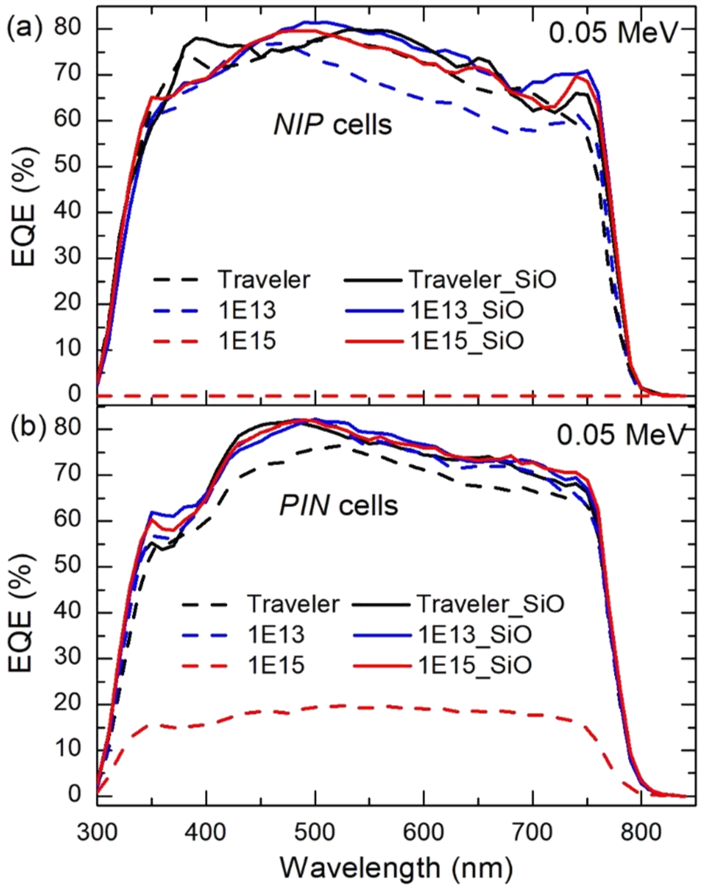

Supplementary Figure 11. EQE spectra on irradiated cells.

EQE data on (A) *NIP*, and (B) *PIN* triple-cation solar cells irradiated with different fluences of 0.05 MeV protons. Data for both bare (dashed lines) and protected (solid lines) are shown.

Supplementary Table 1.

Integrated J_{SC} values for solar cells irradiated with 0.05 MeV protons calculated from EQE spectra shown in Figure S11. EQE spectra were used as supporting evidence to show the changes occur across the whole spectrum rather than for specific wavelengths. Data from AM 1.5G measurements shown in Table 1 is based on an NREL-calibrated Si photodiode provides a more accurate representation of the J_{SC} trends.

Architecture	0.05 MeV proton fluence (cm^{-2})	Int. J_{SC} ($mA.cm^{-2}$)
*NIP*_without SiO_X	10^{13}	16.66
	10^{15}	0
*NIP*_with 1 µm SiO_X	10^{13}	18.86
	10^{15}	18.40
*PIN*_without SiO_X	10^{13}	18.58
	10^{15}	4.56
*PIN*_with 1 µm SiO_X	10^{13}	18.97
	10^{15}	19.02

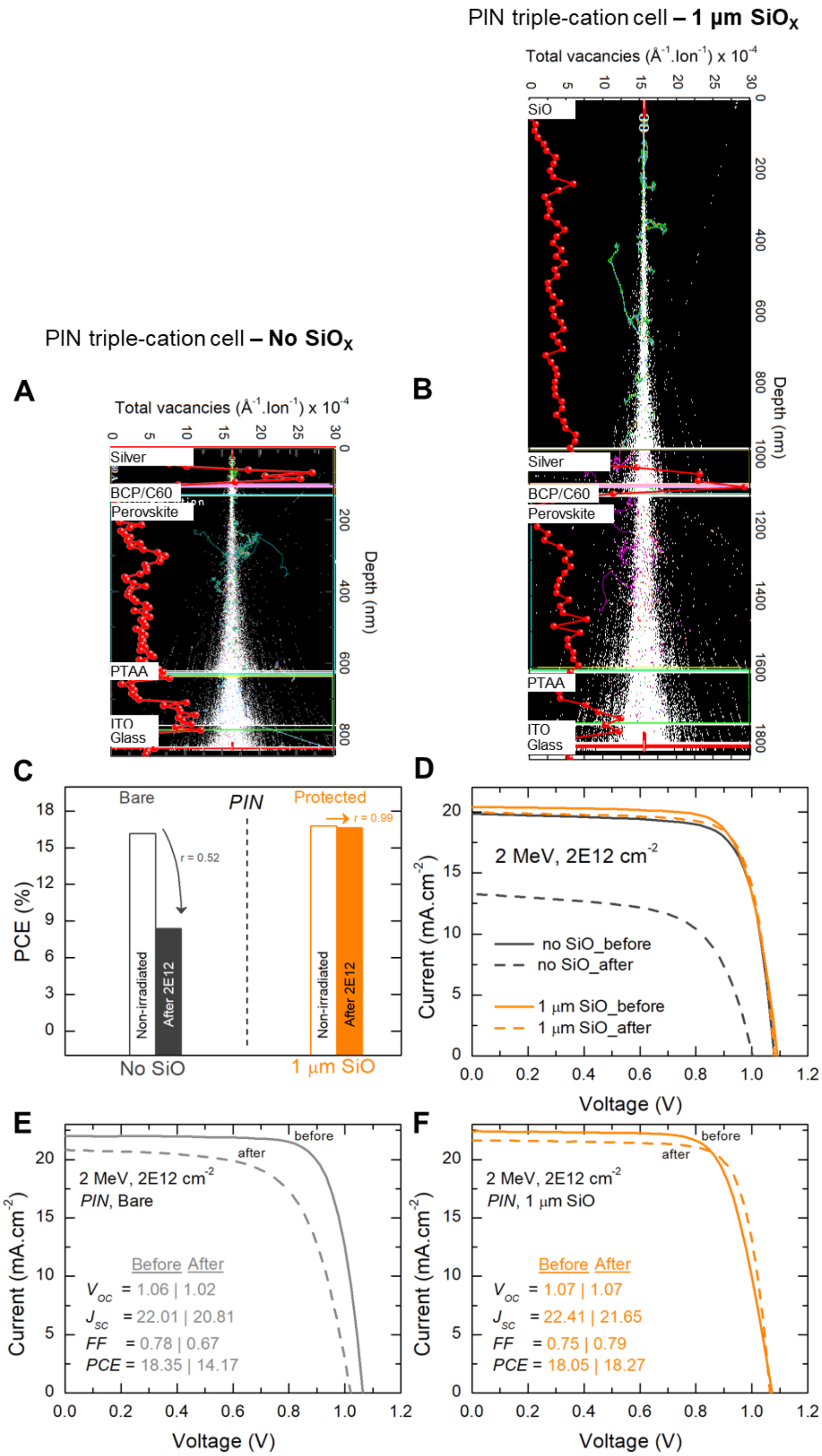

Supplementary Figure 12. SRIM/TRIM simulations for 2.0 MeV α-particles on *PIN* cells. *α-irradiation of PIN triple-cation cells.* SRIM/TRIM simulations for 2 MeV α-particles incident on a *PIN* triple-cation solar cell (A) without, and (B) with 1 μm SiO_X. (C) Effect of α-irradiation using the RBS setup on the PCEs, and (D) corresponding *J-V* curves. Results of α-irradiation carried out at IBL, University of North Texas are shown in (E) and (F).

Supplementary Note 1: Cumulative DDD and Lifetime calculations

1-year differential proton fluences for the various orbits were obtained by simulating the orbits in SPENVIS.[1] Next, considering the stopping powers of 1 μm SiO_X from SRIM/TRIM, slowed proton fluences were calculated. NIEL values for various proton energies were calculated for the triple-cation solar cells using SPENVIS. NIEL calculations were carried out using SPENVIS and further verified using SR-NIEL.[2] Both codes calculate NIEL of a defined chemistry using a screened relativistic treatment for elastic Coulombic interactions between the incident particles and the target. Besides the chemical composition of the target, these codes require the displacement threshold energy for each element in the target as input parameters. We used the energies from SRIM: C = 28 eV, H = 10 eV, N = 28 eV, O = 28 eV, Cs = 25 eV, Pb = 25 eV, I = 25 eV, Br = 25 eV. In a previous report, we have calculated NIELs for various materials using these codes. Although NIELs for perovskite semiconductors have not yet been published by other researchers, the Si and III-V NIELs we calculated are in full agreement with previously published curves justifying the model used by SPENVIS and SR-NIEL.

Cumulative DDD was calculated as follows:

Cumulative displacement damage dose for a given orbit, $\int DDD = \int N_P(E) \cdot NIEL(E) \cdot dE$, over the entire proton energy range for that orbit, where $N_P(E)$ is the fluence of protons at energy E, and $NIEL(E)$ is the proton NIEL at energy E, as described in Messenger et al.[3]

Lifetime in the orbit can then be calculated by computing the DDD for the particle energy E_0 used for irradiation, $DDD(E_0) = N_P(E_0) \cdot NIEL(E_0)$, and dividing it by $\int DDD$

Lifetime (years) = $DDD(E_0)/\int DDD$

For example, 0.05 MeV proton irradiation at a fluence of 10^{13} cm^{-2} results in a dose, $DDD(0.05\ p)$ = 3.9E12 $MeV.g^{-1}$, and corresponds to 0.06 years in GEO which has a $\int DDD$ of 6.57E13 $MeV.g^{-1}$.

Since the SiO_X layer fully blocks the 0.05 MeV protons, we sought to irradiate the solar cells with fully-penetrating protons to calculate the device's lifetime in orbit. We are specifically interested in quantifying the impact of those fully penetrating particles that do not simultaneously cause healing. High-energy fully penetrating protons have been shown to cause healing and increase in device performance due to the higher ionizing energy loss (IEL) associated with them.[4,5] In general, particles with a lower value of IEL/NIEL ratio should be used for testing the radiation tolerance of perovskite solar cells. Figure S8 compares the IEL/NIEL ratio for 2 MeV protons and 2 MeV α-particles. Given their larger mass, α-particles are the most damaging radiation in space with a lower IEL and significantly higher NIEL values than protons, resulting in a relatively lower IEL/NIEL ratio. We therefore considered 2 MeV α for the lifetime calculation. 2 MeV α-particles at a fluence of 2.0×10^{12} cm^{-2} with DDD (2.0 α) = 7.8×10^{11} MeV.g^{-1} led to a 50% degradation in device performance, while the SiO_X-capped cells retained 90% of their original PCE after irradiation with 2.0×10^{13} cm^{-2} fluence of 2 MeV α-particles. DDD for various particle energies and fluences are shown in Table S1 and the resulting increase in device lifetimes for various orbits is summarized in Table S2.

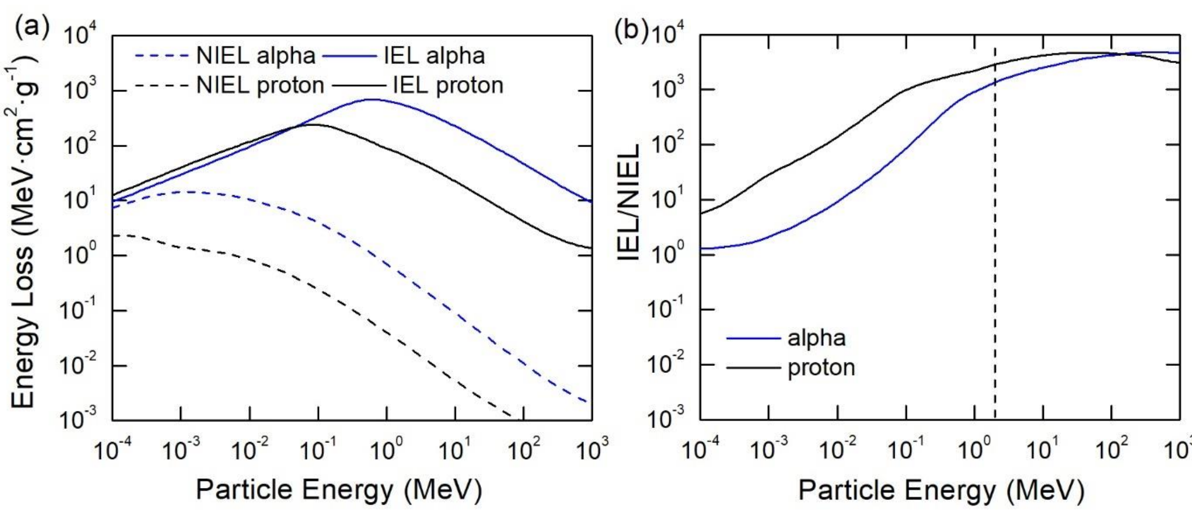

Supplementary Figure 13. NIEL and IEL profiles for protons and α-particles.
(A) NIEL and IEL for protons (black) and α-particles (blue) calculated for various particle energies using SR-NIEL.[2] (B) IEL/NIEL ratio for protons (black) and α-particles (blue). The dashed line indicates 2 MeV.

Supplementary Table 2.
DDD for various particle energies and fluences.

DDD ($MeV.g^{-1}$)	Fluence (cm^{-2})			
	10^{12}	10^{13}	10^{14}	10^{15}
0.05 p^+	3.9E11	3.9E12	3.9E13	3.9E14
2.0 α^+	3.9E11	3.9E12	3.9E13	3.9E14

Supplementary Table 3.
Cumulative DDD for the bare and SiO_X protected devices, and the calculated lifetimes.

	LEO (ISS)	LEO (2000 km)	5000 km	GEO	Juno
$\int DDD$ – bare	2.76E9	2.65E12	3.48E13	6.57E13	7.29E11
$\int DDD$ – 1 μm SiO_X	1.65E9	1.34E12	1.80E13	1.85E13	6.29E11
Reduction in $\int DDD$	40%	49%	48%	72%	14%
Lifetime bare cell(years)	282.61	0.29	0.02	0.01	1.07
Lifetime 1 μm SiO_X cell (years)	4727.27	5.81	0.43	0.42	12.40

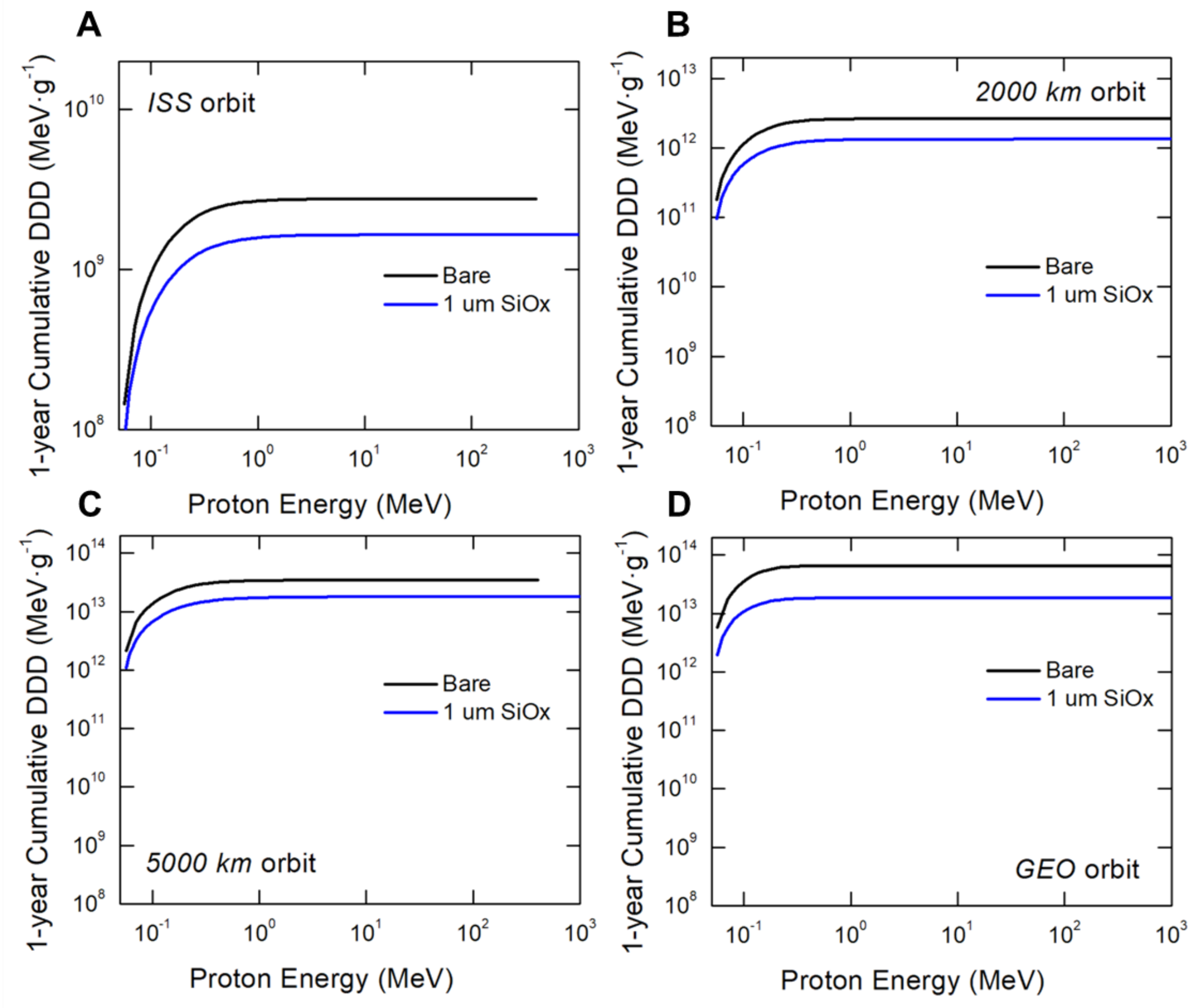

Supplementary Figure 14. Cumulative DDD calculations for various orbits.
1-year cumulative DDD for various orbits comparing the cases of a bare (black) and 1 μm SiO_X protected (blue) solar cells.

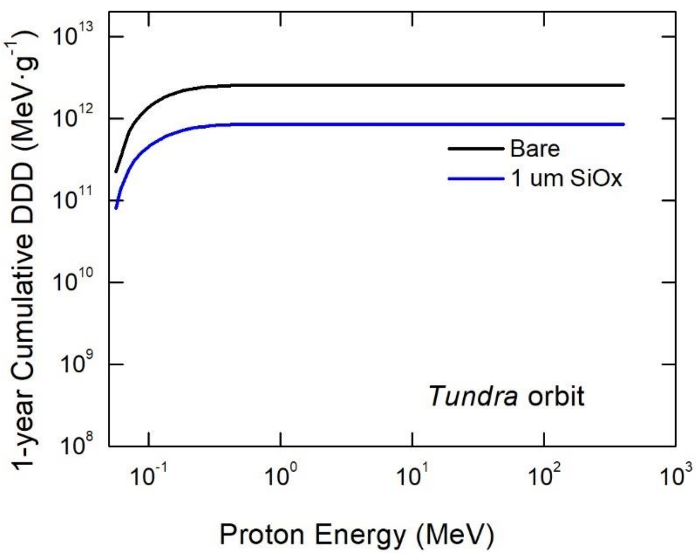

Supplementary Figure 15. Cumulative DDD calculation for the Tundra orbit.
1-year cumulative DDD for the Tundra orbit comparing the cases of a bare (black) and 1 µm SiO_X protected (blue) solar cells.

Supplementary Table 4.
Cumulative DDD for the bare and SiO_X protected devices, and the calculated lifetime for the Tundra orbit.

	Tundra
∫*DDD* – bare	2.49E12
∫*DDD* – 1 um SiO_X	7.97E11
Reduction in ∫*DDD*	68%
Lifetime bare cell(years)	0.31
Lifetime 1 µm SiO_X cell (years)	9.79

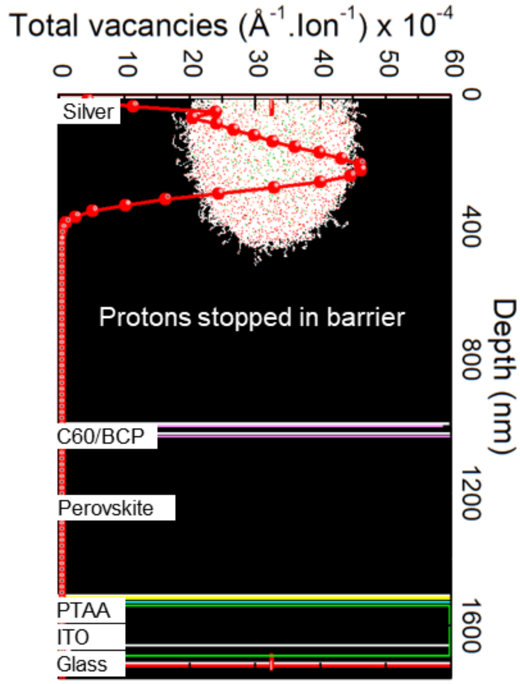

Supplementary Figure 16. SRIM/TRIM simulation on a 1000 μm Silver capped PIN cell. SRIM/TRIM simulation on a perovskite solar cell capped with a 1000 μm barrier of Silver. Simulation was carried out for 0.05 MeV protons and all protons were found to be blocked within 300 nm of the barrier.

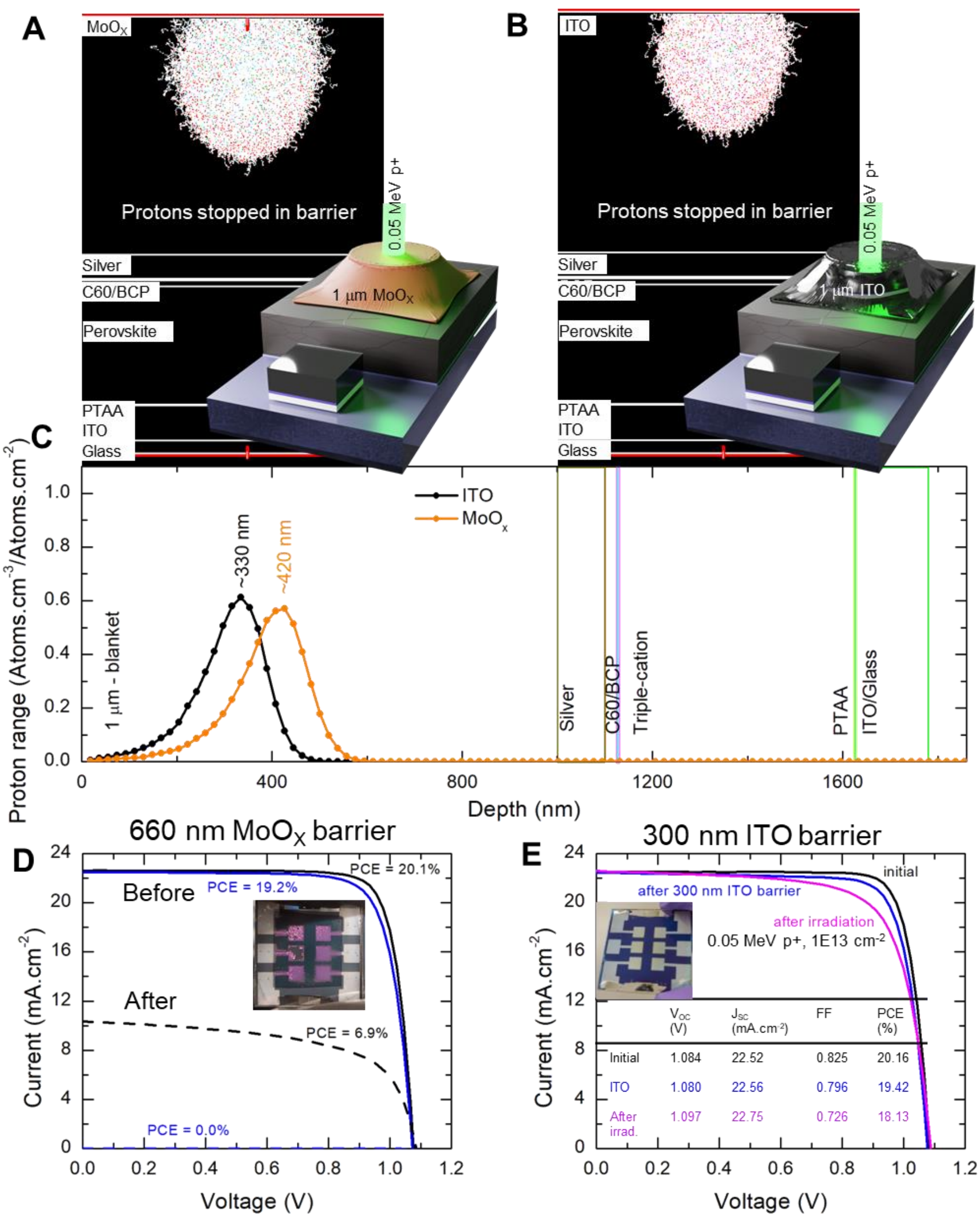

Supplementary Figure 17. SRIM/TRIM simulations for MoO_X and ITO barriers.
SRIM/TRIM simulations showing straggling of 0.05 MeV protons in 1 um barriers of (A) MoO_X, and (B) ITO atop perovskite solar cells. (C) Proton ranges are found to be 420 nm and 330 nm in MoO_X and ITO, respectively. These layers were deposited via thermal evaporation (MoOx) and sputtering (ITO). (D) While significant device degradation was observed for MoO_X, (E) ITO barrier only resulted in a slight performance drop.

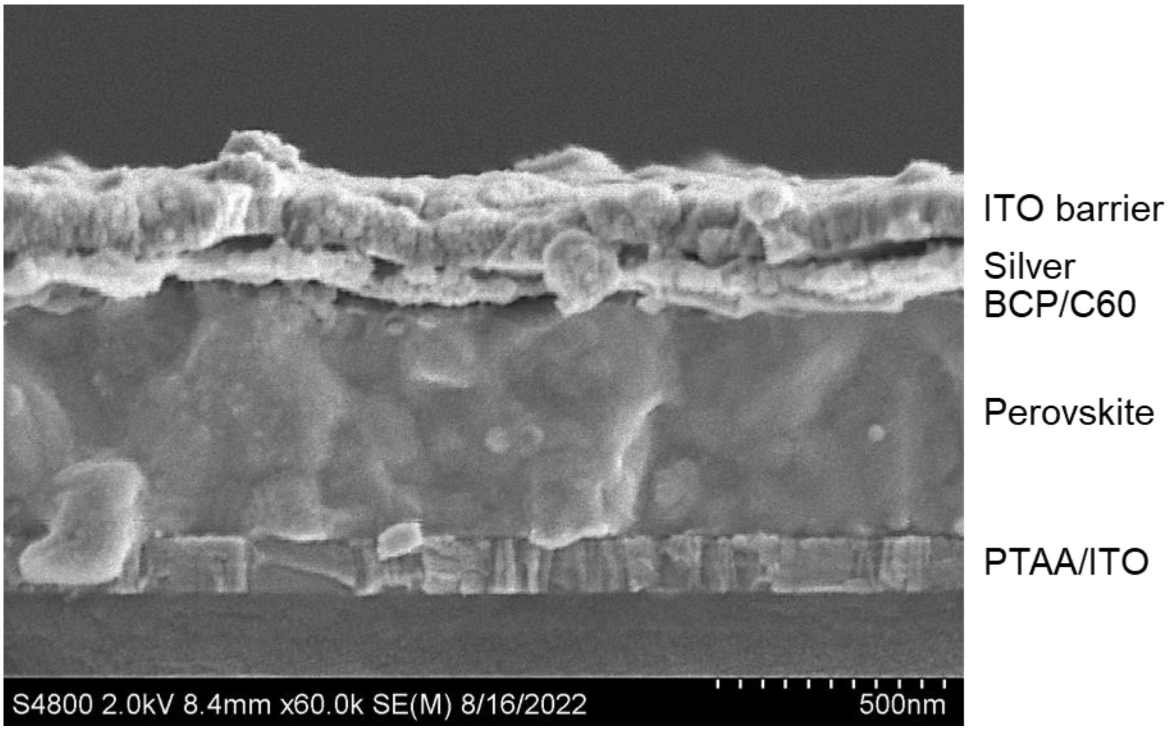

Supplementary Figure 18. X-SEM of a cell with ITO barrier.
X-SEM image showing a less uniform ITO barrier as compared to SiO_X shown in Figure 1D.

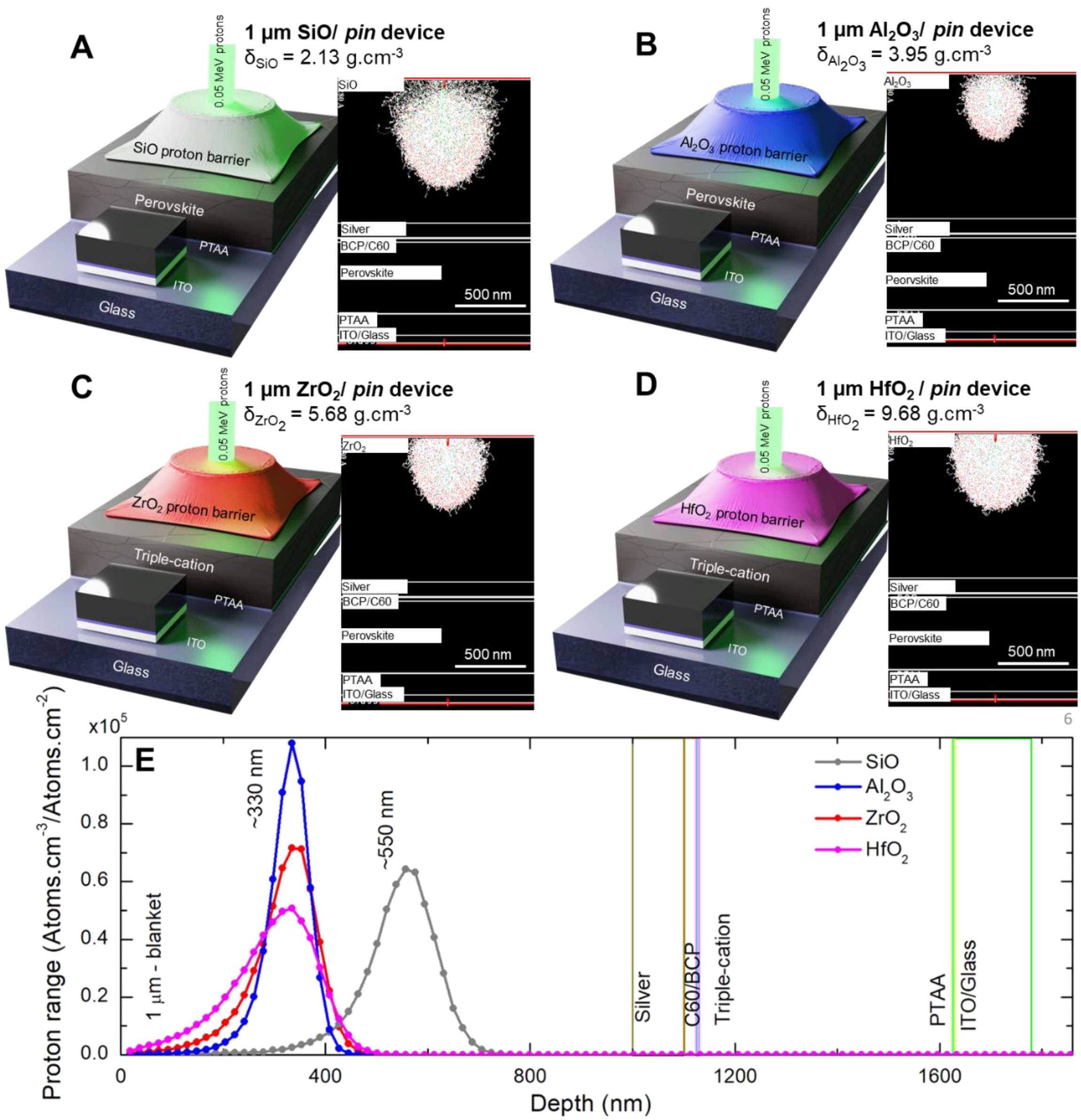

Supplementary Figure 19. SRIM/TRIM simulations for various oxide barriers.
Oxide barrier library: Simulated proton straggling for various 1 μm thick oxide proton barriers on *PIN* triple-cation devices. Proton ranges for each case are shown in (E).

Supplementary Table 5.
Comparison of the metal oxide barriers proposed and simulated in this work besides the experimentally explored SiO_X, MoO_X, and ITO.

Oxide	Deposition	Temperature	Rate	0.05 MeV Proton stopping range	Availability in standard processing
Al_2O_3	ALD/e-beam	~80-90 °C	~0.4-0.8 $nm.min^{-1}$	~330 nm	Common
ZrO_2	ALD/e-beam	~80-90 °C	~0.4-0.8 $nm.min^{-1}$	~340 nm	Rare
HfO_2	ALD/e-beam	~80-90 °C	~0.4-0.8 $nm.min^{-1}$	~330 nm	Rare

Supplementary References:

1 https://www.spenvis.oma.be/.
2 https://sr-niel.org/.
3 Messenger, S. R., Summers, G. P., Burke, E. A., Walters, R. J. & Xapsos, M. A. Modeling solar cell degradation in space: A comparison of the NRL displacement damage dose and the JPL equivalent fluence approaches†. *Progress in Photovoltaics: Research and Applications* **9**, 103-121, doi:https://doi.org/10.1002/pip.357 (2001).
4 Durant, B. K. *et al.* Tolerance of Perovskite Solar Cells to Targeted Proton Irradiation and Electronic Ionization Induced Healing. *ACS Energy Letters* **6**, 2362-2368, doi:10.1021/acsenergylett.1c00756 (2021).
5 Brus, V. V. *et al.* Defect Dynamics in Proton Irradiated CH3NH3PbI3 Perovskite Solar Cells. *Advanced Electronic Materials* **3**, 1600438, doi:https://doi.org/10.1002/aelm.201600438 (2017).